J. Appl. Comput. Mech., 5(4) (2019) 749-762
DOI: 10.22055/JACM.2019.27528.1414

ISSN: 2383-4536
jacm.scu.ac.ir

M&MoCS
Shahid Chamran University of Ahvaz

Journal of
Applied and Computational Mechanics

Research Paper

Numerical Modeling and Multi Objective Optimization of Face Milling of AISI 304 Steel

K. Krishnaprasad[1], C.S. Sumesh[2], A. Ramesh[3]

[1] Department of Mechanical Engineering, Amrita school of Engineering, Coimbatore, Amrtia Vishwa Vidyapeetham, India, Email: kpk1110@gmail.com
[2] Department of Mechanical Engineering, Amrita school of Engineering, Coimbatore, Amrtia Vishwa Vidyapeetham, India, Email: cs_sumesh@cb.amrita.edu
[3] Department of Mechanical Engineering, Amrita school of Engineering, Coimbatore, Amrtia Vishwa Vidyapeetham, India, Email: r_ajith@cb.amrita.edu

Received November 07 2018; Revised January 06 2019; Accepted for publication February 08 2019.
Corresponding author: C.S. Sumesh, cs_sumesh@cb.amrita.edu

Abstract. There is a requirement to find accurate parameters to accomplish precise dimensional accuracy, excellent surface integrity and maximum MRR. This work studies the influence of various cutting parameters on output parameters like Cutting force, Surface roughness, Flatness, and Material removal rate while face milling. A detailed finite element model was developed to simulate the face milling process. The material constitutive behavior is described by Johnson-Cook material model and the damage criteria is established by Johnson-Cook damage model. The result indicate significant effects of all three cutting parameters on MRR and both feed rate and depth of cut have significant effect on cutting force. Also, feed rate has significant effect on PEEQ and none of the parameters have effect on flatness.

Keywords: Face Milling, AISI 304 Steel, Surface Roughness, Flatness, Material Removal Rate, Response Surface Methodology.

1. Introduction

Milling is a material removing process, in which a rotating cutting tool is used to remove material from workpiece. In Face milling process the cutter axis is perpendicular to machining surfaces. In face milling, feed is given either horizontal or vertical directions, also it can produce flat surfaces and machines work to the required length. In this work AISI 304 steel used.

AISI 304 steel has good corrosion resistance to various environments and also has good heat resistance. Moreover it can be used in fusion welding and can be cold worked to increase hardening, and it also has good machinability. Because of these properties 304 steel is generally used in nuts, bolts, springs, screws, sanitary ware and troughs, architectural paneling, cutlery and flatware, tubing etc.

Kannan et al. [1] examined the influence of spindle speed, feed rate (f) and cutting depth on MRR and Ra of face milling operation on copper work piece using hybridization of RSM with genetic algorithm. Prajapati et al. [2] investigated the impact of feed rate (f), spindle speed (N), and cutting depth on MRR and Ra during end milling of aluminum alloy using Taguchi method. Yasir et al. [3] studied the influence of feed rate (f) and spindle speed on Ra during milling of AISI 316L steel and optimized the process using RSM. Shaik and Srinivas [4] studied the effect of parameters like feed rate (f), spindle speed, and cutting depth on tool vibration and Ra while milling Al 6061 alloy. Optimization was done by using Box-Behnken design method. Balasubramanyam et al. [5] considered the influence of cutting depth, spindle speed, helix angle, and feed rate (f) on Ra during end milling process of SS 202. CCD in RSM is used for this study. Vijay and Krishnaraj [6] examined the importance of spindle speed (N), cutting depth, feed rate (f) on cutting force (Fc) and surface finish while end milling of Ti-6Al-4V alloys. The output parameters were optimized using Taguchi and ANOVA. Rameshkumar et al. [7] have monitored tool conditions using acoustic emission and vibration signatures, during high speed milling of titanium alloy (Ti-6Al-4V). Also, to predict the tool conditions, algorithms like Decision tree, Artificial Neural Networks and Support Vector Machine were used to envisage the tool condition.

Published online: May 09 2019

Kumar and Paswan [8] studied the influence of spindle speed (N), cutting depth and feed on tool wear and surface finish while end milling of AISI 413 steel. Optimization of process parameters was done by RSM. Ninase and Khodke [9] examined the effect of cutting depth, spindle speed and feed rate (f) on surface finish during end milling of Al 7075 alloy. L8 orthogonal array (OA) was used in the research. Wathore and Advanib [10] investigated the influence of spindle speed (N), cutting depth and feed rate (f), on Ra and MRR while end milling of H13 Die steel. Grey relational analysis based on Taguchi, was used in the study for optimization of the process. Kumbhar et al. [11] have done multi-objective optimization of CNC end milling operation, considering spindle speed (N), cutting depth and feed rate (f) as machining factors and Ra and MRR as response parameters. Taguchi L9 OA was used for the optimization purpose. Marimuthu et al. [12] have proposed a mathematical model to envisage the residual stresses in milling process using statistical techniques.

Rawangwong et al. [13] optimized the cutting conditions using RSM, for face milling of Al semi solid 2024 alloy. Spindle speed, cutting depth and feed rate (f) were selected as the machining parameters and Ra was the response parameter. Rawang et al. [14] examined the influence of cutting depth, spindle speed (N) and feed rate (f) on Ra while face milling operation of AA 7075 alloy. Lakshmi and Subbaiah [15] studied the influence of input variables like cutting depth, spindle speed (N) and feed rate (f) on Ra and MRR while end milling of EN24 steel. Process optimization was done by using RSM. Shelar and Shaikh [16] investigated the influence of spindle speed (N), cutting depth and feed rate (f), on Ra, MRR, dimensional accuracy and flatness during CNC milling operation of AISI 316 stainless steel. Pramod et al. [17] have developed an orthogonal, coupled thermo - mechanical analysis using numerical model to envisage the surface residual stresses during milling operation of AISI 1045 steel using HSS tool.

Subramanian and Veerapriya [18] investigated the influence of cutting depth, spindle speed (N) and angle on MRR and Ra during end milling of AISI 4340 steel. Sheth and George [19] have experimentally examined the influence of feed rate (f), spindle speed (N) and cutting depth on flatness and Ra during face milling of wrought cast steel grade B material. Moaz et al. [20] developed a detailed finite element model to study the effect of feed rate (f) on Ra and cutting force (Fc) in face milling of Ti-6Al-4V alloys. Krishna Kumar et al. [21] have a developed a three dimensional FE model to envisage residual stresses during end milling of Ti-6Al-4V alloy. Ramesh et al., [22] presented a detailed finite element model to predict deformation and other machining characteristics involved in high-speed orthogonal machining (cutting speed > 54 m/min) of hard-to-deform materials like Ti6Al4V. The influence of various cutting parameters like feed rate, spindle speed, and rake angle, on the output parameters like cutting force and surface finish, were analyzed. Sumesh and Ramesh [23] studied the influence of machining parameters, Cutting Speed, Feed Rate, and Depth of cut, on surface finish during dry orthogonal turning of Al 6061 – T6 alloy, is studied using the response surface methodology (RSM).

Reimer et al. [24] established a 3D FE-model for modelling precision end milling process with a two-flute ball nose cutter. A subroutine was implemented to model work piece hardening during the cutting process. Ducobu et al. [25] studied the implementation of the Coupled Eulerian-Lagrangian (CEL) method in Ti6Al4 V orthogonal cutting. This method to combines the Lagrangian and Eulerian techniques without any element deformation problem. Rezaei et al. [26], determined of the minimum uncut chip thickness experimentally during micro-end milling of titanium alloy Ti-6Al-4V with respect to influences of cutting parameters and lubricating systems. Aydın and Köklü [27] evaluated the effectiveness of FE modeling for estimating the cutting forces in ball-end milling process using two different finite element (FE) models with Arbitrary Lagrangian Eulerian (ALE) techniques. Peng et al. [28], carried temperature and deformation measurement test during micro – machining tests based on the theoretical model of temperature field distribution of workpiece and the simulation model of workpiece deformation. The influence of cutting heat and cutting force on the machining precision of micro-machining were studied. Gao et al. [29], presented a 3D coupled Eulerian-Lagrangian (CEL) finite element method (FEM) model for the simulation of end milling processes based on Abaqus/Explicit. Pittalà and Monno [30] modelled the milling operation three-dimensionally, considering the real geometry of the insert. 3D DEFORM was used to carry out the FEM simulations. Krasauskas et al. [31] investigated the experimental analysis and numerical simulation of the stainless AISI 304 steel friction drilling process. They obtained the variations of experimental axial force and torque values and compared to finite element simulation results and concluded that the presumptions taken in the simulation are correct and realistically define the friction drilling process.

Pimenov and Guzerv [32] studied the tension forces on the tools flank surface during orthogonal cutting, using a finite element model. Pimenov [33] analyzed the changes in the profile of machined surface at micro level while face milling of steel-45 workpiece. Pimenov et al. [34] proposed a novel method to determine the deviation in angular values of GF 217155 milling system. It also evaluates deviation in flatness for different values of flank wear. Grzenda and Bustillo [35] investigated how the missing product features can contribute to the development of prediction models. Rodriguez et al [36] presented a soft computing technique based on decision making for the accurate prediction of roughness in terms of tool wear and tool type. Wojciechowski et al. [37] developed a method to minimize the vibration and cutting forces during precise ball end milling of hardened steel, by optimizing surface inclination angle and tools overhang. Wojciechowski et al. [38] proposed a novel experimental method to estimate milling machine vibrations caused by milling forces. Wojciechowski et al. [39] proposed a multi criteria optimization method for reducing the cutting force and improving efficiency while ball end milling of hardened steel.

The present work is used to accurately predict and optimize output parameters during Face Milling of AISI 304 Steel in a conventional vertical milling centre. The output parameters considered in this study are; Cutting force (Fc), Ra, flatness, and MRR. In this present paper, a detailed two dimensional FE model of face milling process is developed. This aims to study the influence of milling parameters like cutting depth, spindle speed (N) and feed rate (f) on MRR, cutting force (Fc), Ra, flatness during face milling of AISI 304 steel. The material constitutive behavior is described by Johnson-Cook (JC) material model and the damage criteria is established by Johnson-Cook (JC) damage model. Dynamic explicit analysis was used in the development of the model. Also ALE method was used to precisely envisage the flow of material while milling. ANOVA and RSM are used to determine the significance of milling factors on output variables. Optimization of each response variable is done using RSM and a quadratic response surface model was developed for each response. Using the model developed by RSM all the response parameters have been optimized.

2. Introduction to Response Surface Methodology

The RSM is a statistical data processing method based on experimental design and a number of experimental data, which uses multivariable linear or quadratic regression equations to fit the functional relationship between the response and the experimental factors to establish a mathematical model. The response surface method finds out the relation model between the variables and the response in the way of the fitting surface. Industrial problems can be conveniently modeled by RSM, which is a combination of statistical tools and mathematical methods. It is commonly used for optimizing manufacturing problems in which the response is effected by many factors. RSM uses economical, systematic, practical and easy method to get optimal parameters. RSM is one of the techniques for obtaining the best or optimum conditions. The workpiece material used in this study is AISI 304 steel. Its chemical composition is shown in Table 1.

Table 1. Chemical Composition of AISI 304 steel

Component	C	Cr	Fe	Mn	Ni	P	S	Si
Weight %	Max. 0.08	18-20	66.345-74	Max. 2	8-10.5	Max. 0.045	Max. 0.03	Max. 1

In the current work, the selected milling parameters are cutting depth (doc), feed rate (f) and spindle speed (N) and the considered output responses are cutting force (Fc), Ra (PEEQ), flatness (F) and material removal rate (MRR). RSM based on CCD was used to for analysis and optimization. The parameters and their associated levels are selected from the possible ranges of machine tool, on which experiments were conducted and are given in Table 2.

Table 2. Milling parameters and the levels

Parameters	Level-1	Level-2	Level-3
Cutting speed/ Spindle speed N, (rpm)	500	750	1000
Feed rate f , (mm/min)	63	131.5	200
Cutting depth/depth of cut doc, (mm)	0.5	1.0	1.5

Design of experiments software was used to get a set of trials for the analysis of input parameters and their effects on output parameters while face milling. Using CCD and above selected levels of parameters, 20 different combinations were obtained from the software as shown in Table 3.

3. Numerical Modelling of Face Milling Process

In the present work, a detailed 2D numerical model was developed for face milling process of AISI 304 steel to envisage the effect of selected milling parameters on the response parameters using ABAQUS/Explicit. The tool is made to be analytically rigid body with clearance angle less than 20^0 and rake angle to be $0^{0.}$ Whereas the work piece is made to be a deformable body. The Fig. 1 shows the finite element modeling of face milling process. The length and width dimensions shown in Fig. 1 are taken based on Chen et al. [40]. In the finite element modelling, an Adaptive Lagrangian-Eulerian technique (ALE), for describing the work piece flow and element deletion was used. In the model proposed, Lagrangian technique is used on regions far away from the tool and Eulerian approach is used in the cutting zone. A mesh convergence study was performed and were obtained the results with in the limit, less than 5% (3.46%).

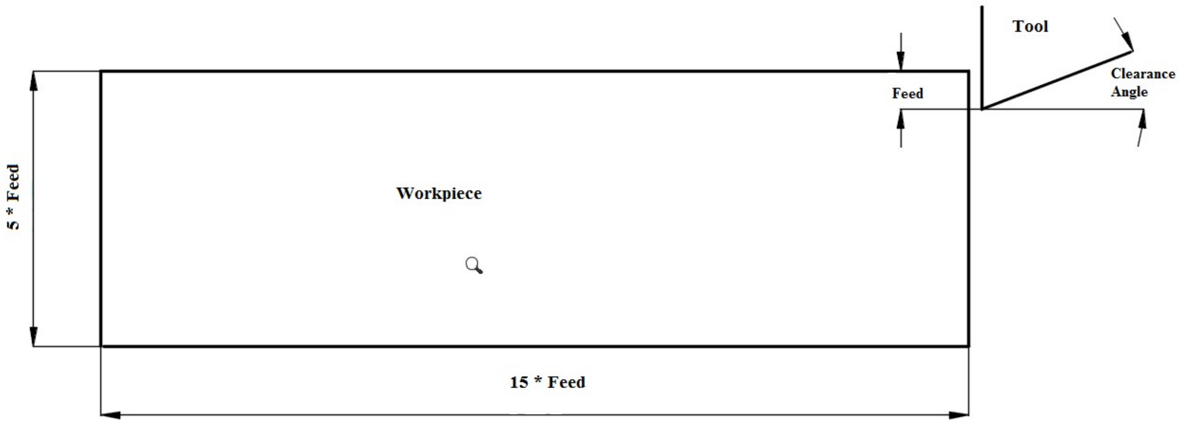

Fig 1. Work piece-tool assembly

By conversion of the face milling process from 3D to 2D the original cutting depth becomes the out of plane thickness and the feed (f) becomes the cutting depth in 2D milling operation, the spindle speed (N) becomes the tool velocity. After doing the mesh convergence study, 11224 elements and 11470 nodes were used in the model. In this FE model, the material constitutive behavior is described by Johnson-Cook (JC) material model. It is represented by Eq. (1) [41].

$$\bar{\sigma} = \left[A + B\left(\bar{\varepsilon}_{pl}\right)^{n}\right]\left[1 + C\ln\left(\frac{\dot{\varepsilon}_{pl}}{\dot{\varepsilon}_{0}}\right)\right]\left[1 - \left(\frac{T - T_{room}}{T_{melt} - T_{room}}\right)^{m}\right] \tag{1}$$

Table 3. 20 combinations and simulation results

Trials	Spindle speed N (rpm)	Feed rate f (mm^3/min)	Cutting depth/doc (mm)	Cutting force Fc (N)	Flatness (*10^{-3}mm)	PEEQ	M.R.R (mm^3/sec)
1	500	200	1.5	6457.515	0.039742	0.730899	8267.667
2	750	131.5	1	3190.686	0.06694	0.884256	5490.431
3	500	63	1.5	2735.568	0.018005	1.047806	2590.391
4	750	200	1	4961.133	0.04201	0.768554	8272.424
5	1000	131.5	1	3048.303	0.054272	0.928186	7287.18
6	1000	200	0.5	2661.039	0.039583	0.754429	5510.44
7	750	131.5	0.5	1692.498	0.075014	0.886459	2741.791
8	500	63	0.5	877.3381	0.013413	1.061923	864.8801
9	500	131.5	1	3449.496	0.019753	0.83055	3605.388
10	750	131.5	1	3190.686	0.06694	0.884256	5490.431
11	750	131.5	1	3190.686	0.06694	0.884256	5490.431
12	750	131.5	1	3190.686	0.06694	0.884256	5490.431
13	1000	63	0.5	1086.33	0.046111	1.067885	1731.913
14	1000	63	1.5	3455.817	0.004412	1.069705	5650.564
15	750	131.5	1.5	4528.255	0.054417	0.887215	8235.604
16	750	131.5	1	3190.686	0.06694	0.884256	5490.431
17	750	63	1	1810.407	0.020074	1.082406	2593.035
18	1000	200	1.5	7393.411	0.059727	0.756118	16521.64
19	500	200	0.5	2180.666	0.057397	0.739884	2756.26
20	750	131.5	1	3190.686	0.06694	0.884256	5490.431

The damage criteria established by Johnson-Cook (JC) damage model based on fracture energy was used in this study. Equation (2) represents the damage expression [41]**:**

$$\bar{\varepsilon}_{oi}^{\,f} = \left(D_1 + D_2 \exp D_3 \frac{\sigma_m}{\bar{\sigma}}\right)\left(1 + D_4 \ln\left(\frac{\dot{\varepsilon}_{pl}}{\dot{\varepsilon}_{0}}\right)\right) \times \left[1 + D_5\left(\frac{T - T_{room}}{T_{melt} - T_{room}}\right)\right] \tag{2}$$

Table 4 shows the material properties of AISI 304 steel [31]. The constants in the JC material model and JC damage model are shown in Tables 5 and 6 respectively, [31].

Table 4. Mechanical and Thermal properties of AISI 304 steel

Mechanical		
ρ = 8350 Kg/m^3	E = 207.8 GPa	υ = 0.3
Thermal		
K= 16.2 W/mK	C_p = 0.452 J/g^{0}C	α = 17.8E-6 /^{0}C

Table 5. JC Material Model Parameters

A (MPa)	B (MPa)	C	n	m	T_{room} (^{0}C)	T_{melt} (^{0}C)
280	802.5	0.0799	0.622	1.0	25	1400

Table 6. JC Damage Model Parameters

D_1	D_2	D_3	D_4	D_5
0.69	0	0	0.0546	0

The analysis step is defined as Dynamic, Coupled Temperature-displacement, Explicit, Linear geometric order. CPE4RT elements are utilized in the model. Complex nonlinear analysis involving contact, plasticity and large deformations can be modelled using these elements. The ALE meshing technique in ABAQUS is also utilized for material flows through mesh. Surface to surface interaction is enabled between tool and work piece and penalty contact method with friction coefficient is applied to the model. Both left edge and lower edge of the work piece are fixed using an encastre boundary condition. A velocity type boundary condition is applied on the tool. Simulations were ran for the 20 combinations shown in Table 3, output parameters were measured for each combinations.

4. Results and Discussions

The model validation was performed by comparing the numerical results of the current model with the experimental results obtained from Moaz et al. [20], for three cases. Table 7 shows a comparison of the results obtained from the developed model with that of literature for a constant values of cutting speed of 1000 rpm and a depth of cut of 0.6 mm. The results show good agreement with the literature, with a percentage of variation between 3 to 7%. Finite element simulations were carried out on the developed model and the output parameters like cutting force, PEEQ, flatness and MRR were captured from the FE software Abaqus Explicit and shown in Table 3.

Table 7. Validation of FE results with experimental results from literature [20]

Sl. No.	Feed rate (mm/min)	# Cutting force from experiments (N)	Cutting force from developed numerical model (N)	Error %
1	80	513.31	531.93	3.50
2	120	565.92	590.73	4.20
3	160	621.22	662.99	6.30

The values of output parameters from the simulations shown in Table 3 were analyzed statistically. Full model analysis of variance (ANOVA) was performed at first then non-significant terms were removed. Another ANOVA was performed, after removing insignificant terms to improve the model. Using RSM a mathematical model was developed and its significance was revealed by ANOVA. R^2 value will always lies between +1 and -1. If the value of R^2 is close to 1, means the response variable is very closely related to input parameters. Hence the model can be used to predict the values of output parameters. Various plots like, main effect plot, interaction plot contour plot and surface plots were also obtained to comprehend the influence of milling parameters on the response variables.

4.1. Influence of milling parameters on cutting force (Fc).

ANOVA was done for cutting force (Fc). The predicted R-squared value of 98.80% is in good settlement with adjusted R-squared value of 97.71%. The normal probability graph of residuals for cutting force (Fc) was plotted in Fig 2(a). In this plot, residuals are close to the straight line, which means the residuals are normally distributed.

From the standardized residual plot shown in Fig 2(b), the residuals are dispersed in both +ve and –ve directions and do not shown any obvious design. This suggests that, model is acceptable. And also, there is no cause to uncertain any violation of the independence or constant variance assumptions.

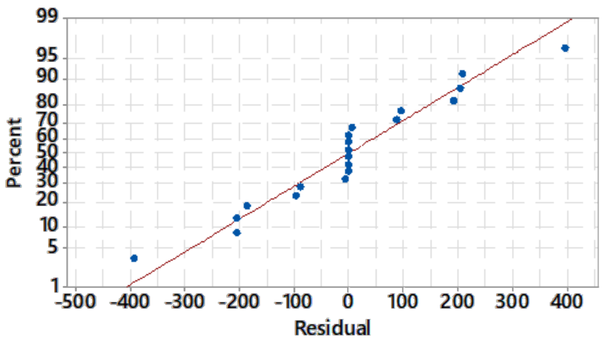

Fig 2(a). Normal probability graph of residuals for cutting force (Fc)

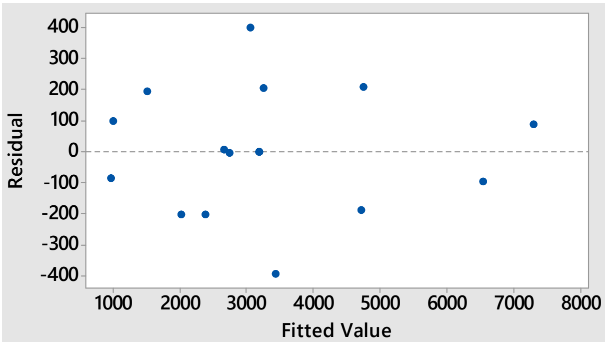

Fig 2(b). Graph of residuals vs. fits for Cutting force (Fc)

Figure 3(a) shows the main effect plot for cutting force (Fc). This plot exhibit data means versus factor levels. Influence of each parameter can be graphically estimated using this plot. In this plot doc and feed rate (f) are the prominent factors. Increase in cutting force (Fc) with feed (f), is because, more material is in contact with tool at unit time. So more force is essential to take away the material. The same reason is applicable to doc also. Figure 3(b) shows the interaction effect plot of cutting force (Fc). The interaction effect of two parameters on cutting force (Fc) is shown in this figure. Figure 3(b) shows that spindle speed (N) X feed rate (f) and spindle speed (N) X cutting depth have some interaction effect on cutting force (Fc).

Figures 4(a) and 4(b) shows 2D contour plot and 3D response plot of cutting force (Fc) for cutting depth and feed rate (f), obtained from DoE software. From Fig. 4, minimum value for cutting force (Fc) occurs at low values of cutting depth and low values of feed rate (f).

Figures 5(a) and 5(b) shows 2D contour plot and 3D response of cutting force (Fc) for cutting depth and spindle speed (N). From Fig. 5, minimum values for cutting force (Fc) occurs at low values of cutting depth and all values of spindle speed (N).

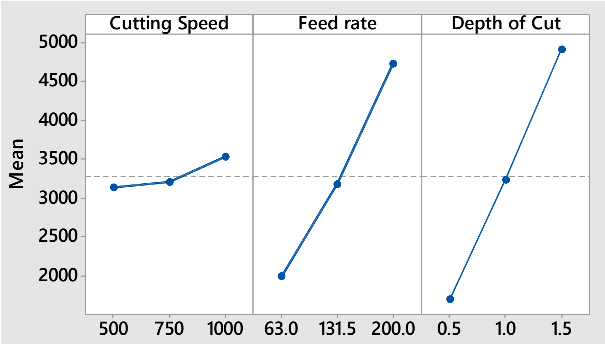

Fig 3(a). Main effect plots for cutting force (Fc)

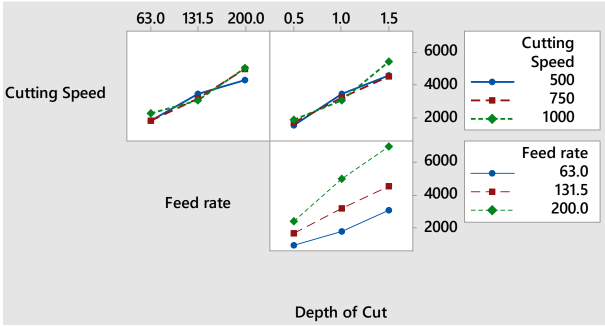

Fig 3(b). Interaction plots for cutting force (Fc)

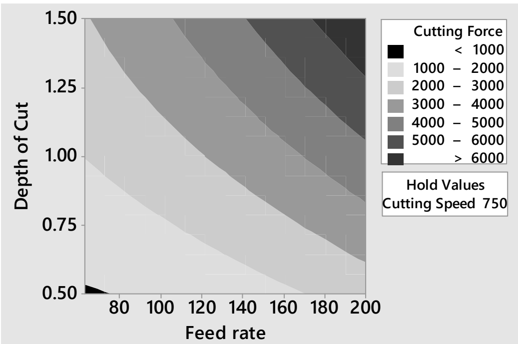

Fig 4(a). Contour plot of cutting force (Fc) for cutting depth vs. feed rate (f)

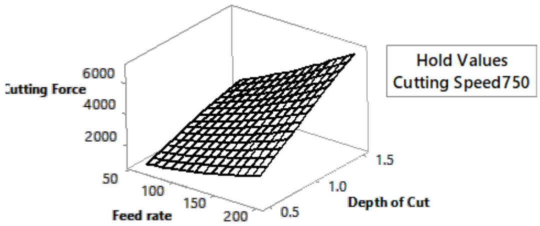

Fig 4(b). Response plot of cutting force (Fc) for cutting depth vs. feed rate (f)

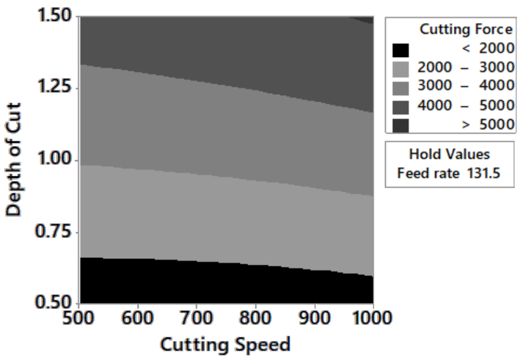

Fig 5(a). Contour plot of cutting force (Fc) for cutting depth vs. spindle speed (N)

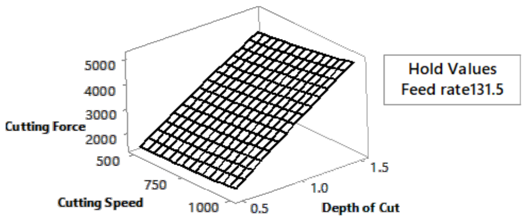

Fig 5(b). Response plot of cutting force (Fc) for cutting depth vs. spindle speed (N)

Figures 6(a) and 6(b) shows 2D contour plot and 3D response plot of cutting force (Fc) for feed rate (f) and spindle speed (N). From Fig. 6, minimum values for cutting force (Fc) occurs at low values of spindle speed (N) and low values of feed (f).

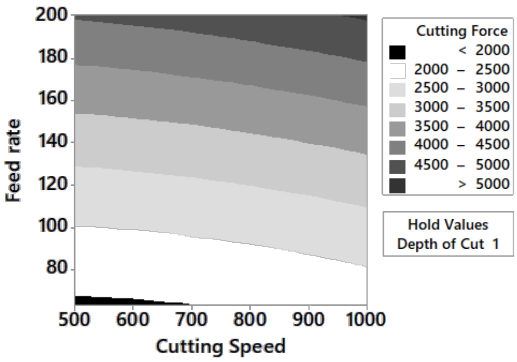

Fig 6(a). Contour plot of cutting force (Fc) for feed vs. spindle speed (N)

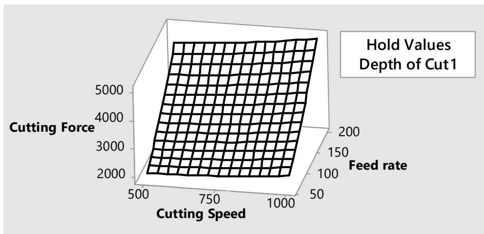

Fig 6(b). Response plot of cutting force (Fc) for feed vs. spindle speed (N)

4.2. Significance of milling parameters on Flatness

Flatness is the waviness of the cutting surface of the work piece. Based on the values of R^2 (79.14%) and adjusted R^2 (60.37%), the model estimated by the regression procedure was found to be significant. The normal probability plot of residuals for flatness was plotted in Fig. 7(a). In this plot, residuals are close to the straight line, which means the residuals are normally distributed.

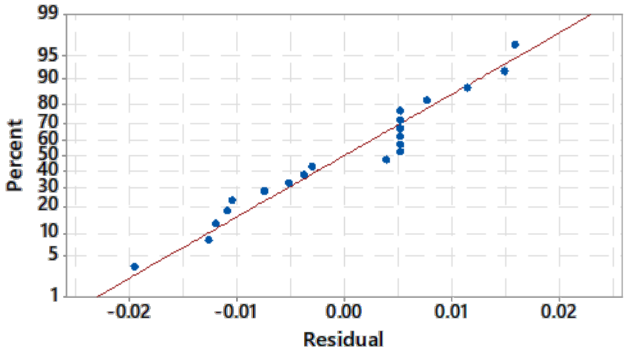

Fig 7(a). Normal probability graph of residuals for flatness

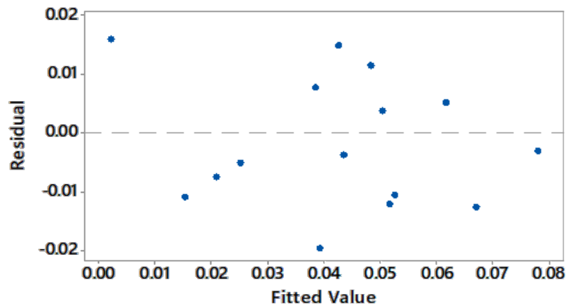

Fig 7(b). Plot of residuals vs. fits for flatness

From the standardized residual plot shown in Fig. 7(b), the residuals are dispersed in both +ve and –ve directions and do not shown any obvious design. This suggests that, model is acceptable. And also, there is no cause to uncertain any violation of the independence or constant variance assumptions

Figure 8(a) shows the main effect plot for flatness. This plot exhibits data means versus factor levels. Influence of each parameter can be graphically estimated using this plot. From this figure, it's difficult to predict which parameter is influencing flatness. Figure 8(b) shows the interaction effect plot for flatness. The interaction effect of two parameters on flatness is shown in this figure. Figure 8(b) shows that spindle speed (N) X cutting depth and feed rate (f) X cutting depth have some interaction effect on flatness.

Figures 9(a) and 9(b) shows 2D contour plot and 3D response plot of flatness for cutting depth and feed rate (f). From Fig. 9, minimum value for flatness occurs at high values of cutting depth and low values of feed rate (f). Figures 10(a) and 10(b) shows 2D contour plot and 3D response of flatness for cutting depth and spindle speed (N). From Fig. 10, minimum values for flatness occurs at high values of cutting depth and low values of spindle speed (N). Figures 11(a) and 11(b) show 2D contour plot and 3D response plot of flatness for feed (f) and spindle speed (N). From Fig. 11, minimum values for flatness occurs at small values of spindle speed (N) and low values of feed (f).

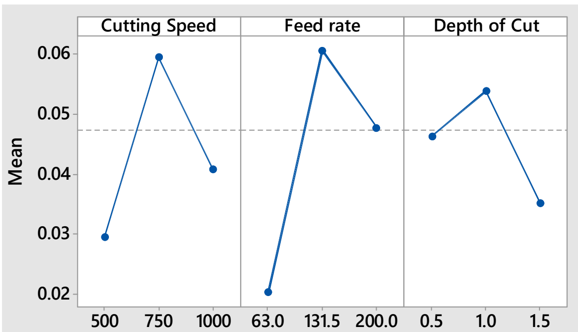

Fig 8(a). Main effect plots for flatness

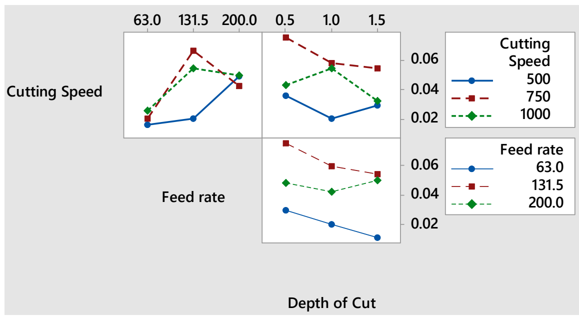

Fig 8(b). Interaction plots for flatness

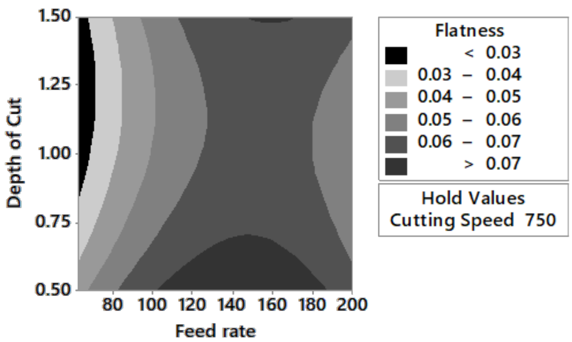

Fig 9(a). Contour plot of flatness for cutting depth vs. feed rate (f)

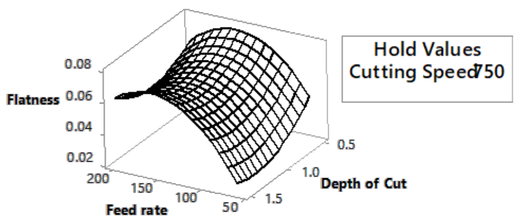

Fig 9(b). Resp. plot of flatness for cutting depth vs. feed rate (f)

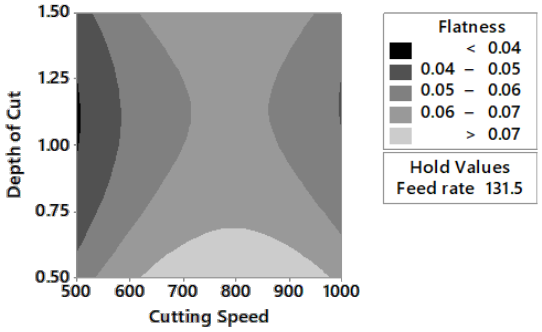

Fig 10(a). Contour plot of flatness for cutting depth vs. spindle speed (N)

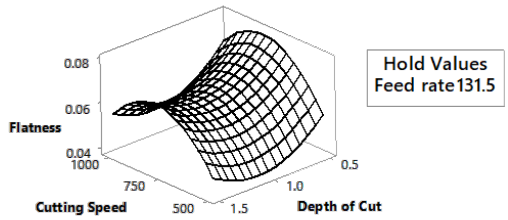

Fig 10(b). Resp. plot of flatness for cutting depth vs. spindle speed (N)

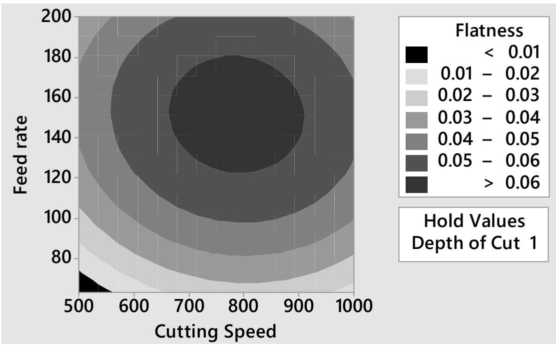

Fig 11(a). Contour plot of flatness for feed vs. spindle speed (N)

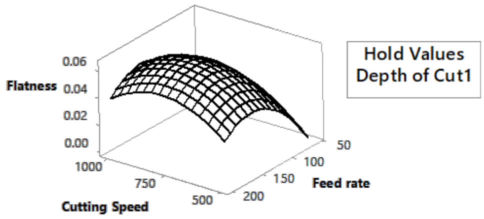

Fig 11(b). Response plot of flatness for feed vs. spindle speed (N)

4.3. Influence of machining parameters on PEEQ

PEEQ is also an important factor to concern since it represents the surface finish of the material. Based on the values of R^2 (98.92%) and adjusted R^2 (97.95%) the model achieved significant results. The normal probability graph of residuals for PEEQ was plotted in Fig. 12(a). In this plot, residuals are close to the straight line, which means the residuals are normally distributed.

From the standardized residual plot shown in Fig. 12(b), the residuals are dispersed in both +ve and –ve directions and do not shown any obvious design. This suggests that, model is acceptable. And also, there is no cause to uncertain any violation of the independence or constant variance assumptions.

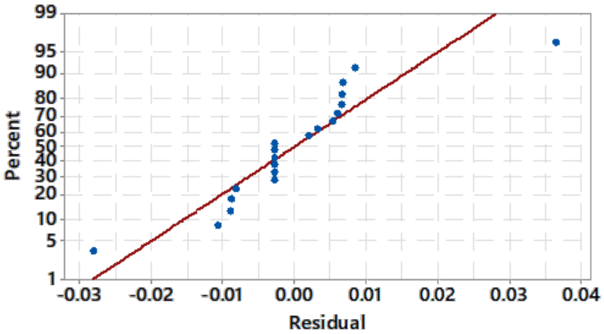

Fig 12(a). Normal probability graph of residuals for PEEQ

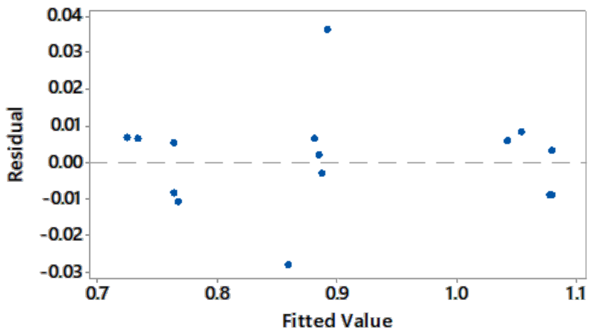

Fig 12(b). Plot of residuals vs. fits for PEEQ

Figure 13(a) shows the main effect plot for PEEQ. This plot exhibits data means versus factor levels. Influence of each parameter can be graphically estimated using this plot. In this figure feed rate (f) is the prominent parameter. Low values of PEEQ mean better surface finish. PEEQ decreases with feed rate (f) because when feed rate (f) increases more volume of material comes in contact with tool at unit time. This means material is removed in faster manner which leads to improved surface finish. Figure 13(b) shows the interaction effect plot of two parameters on PEEQ. Figure 13(b) shows that spindle speed (N) X feed (f) and spindle speed (N) X cutting depth have some interaction effect on PEEQ.

Figures 14(a) and 14(b) shows 2D contour plot and 3D response plot of PEEQ for cutting depth and feed rate (f). From Fig 14, minimum value for PEEQ occurs at all values of cutting depth and high values of feed rate (f). Figures 15(a) and 15(b) shows 2D contour plot and 3D response of PEEQ for cutting depth and spindle speed (N). From Fig 15, minimum values for PEEQ occurs at high values of cutting depth and low values of spindle speed (N).

Figures 16(a) and 16(b) shows 2D contour plot and 3D response plot of PEEQ for feed (f) and spindle speed (N). From Fig. 16, minimum values for PEEQ occurs at small values of spindle speed (N) and high values of feed (f).

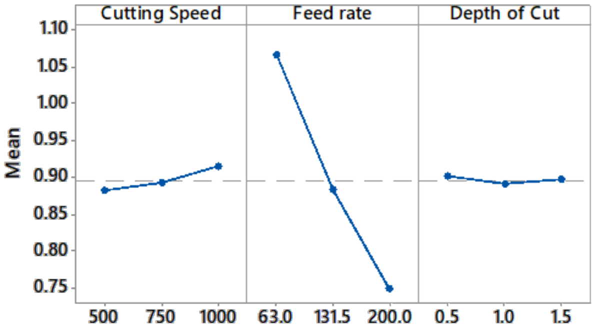

Fig 13(a). Main effect plots for PEEQ

Fig 13(b). Interaction plots for PEEQ

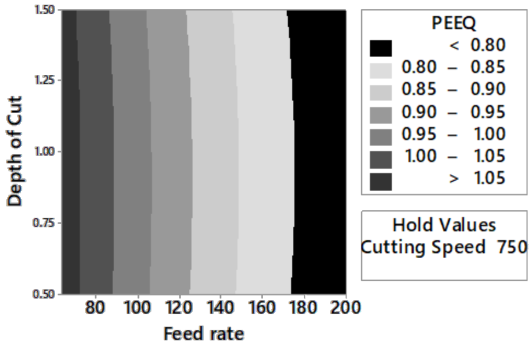

Fig 14(a). Contour plot of PEEQ for cutting depth vs. feed rate (f)

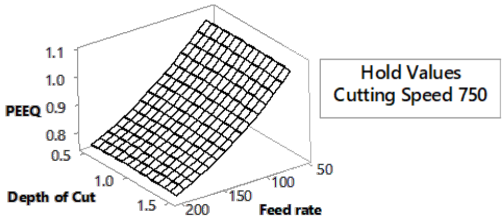

Fig 14(b). Response plot of PEEQ for cutting depth vs. feed rate (f)

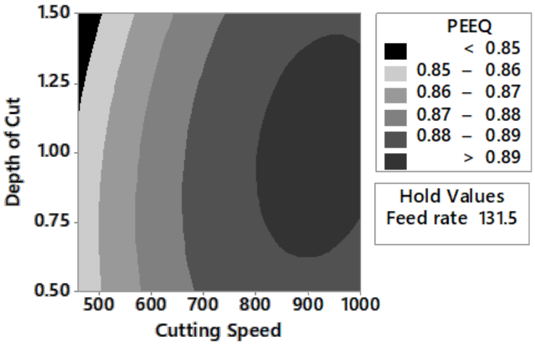

Fig 15(a). Contour plot of PEEQ for cutting depth vs. spindle speed (N)

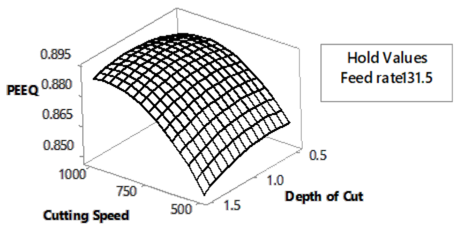

Fig 15(b). Response plot of PEEQ for cutting depth vs. spindle speed (N)

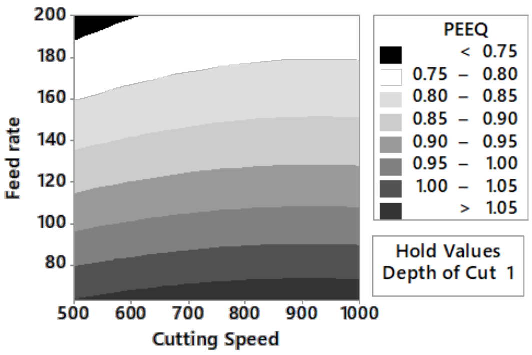

Fig 16(a). Contour plot of PEEQ for feed vs. spindle speed (N)

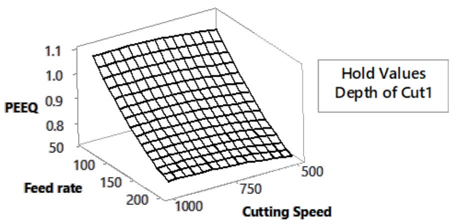

Fig 16(b). Response plot of PEEQ for feed vs. spindle speed (N)

4.4. Influence of machining parameters on MRR

MRR is also a major influential parameter which concerns the industrial economy since it explains the productivity of the machining process. By considering the values of R^2 (99.37%) and adjusted R^2 (98.80%) the model obtained to be significant. The normal probability graph of residuals for MRR was plotted in Fig. 17(a). In this plot, residuals are close to the straight line, which means the residuals are normally distributed.

From the standardized residual plot shown in Fig. 17(b), the residuals are dispersed in both +ve and –ve directions and do not shown any obvious design. This suggests that, model is acceptable. And also, there is no cause to uncertain any violation of the independence or constant variance assumptions.

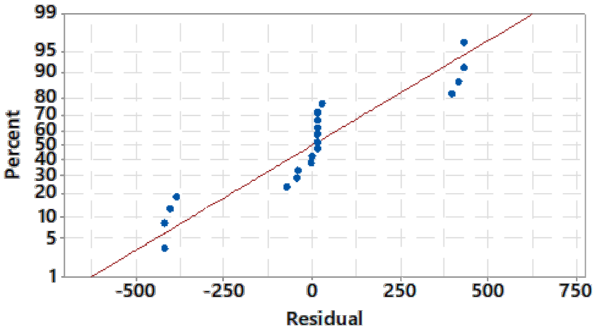

Fig 17(a). Normal probability graph of residuals for MRR

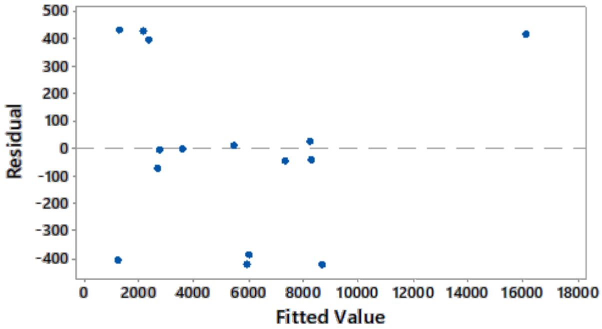

Fig 17(b). Plot of residuals vs. fits for MRR

Figure 18(a) shows the main effect plot for MRR. This plot exhibits data means versus factor levels. Influence of each parameter can be graphically estimated using this plot. In this plot all input parameters have significant effect on MRR. The MRR increases with spindle speed (N) because more volume of material is in contact with tool at unit time. The same reason is applicable to feed (f) and cutting depth also. Figure 18(b) displays the interaction effect plot of MRR. The interaction effect of two parameters on MRR is shown in this figure. In this figure, all the lines are almost parallel to each other which means that there is not much interaction between the parameters.

Figures 19(a) and 19(b) shows 2D contour plot and 3D response plot of MRR for cutting depth and feed rate (f). From Fig. 19, maximum value for MRR occurs at high values of cutting depth and high values of feed rate (f).

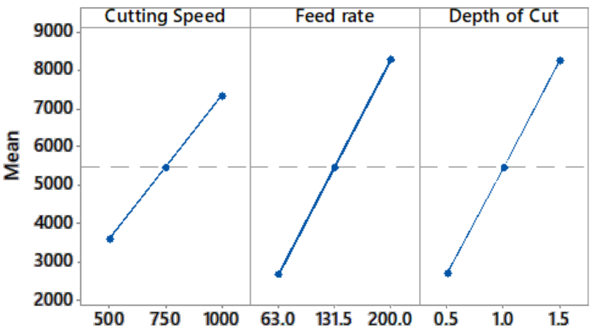

Fig 18(a). Main effect plots for MRR

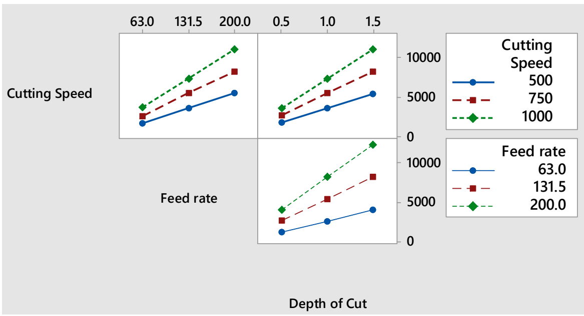

Fig 18(b). Interaction plots for MRR

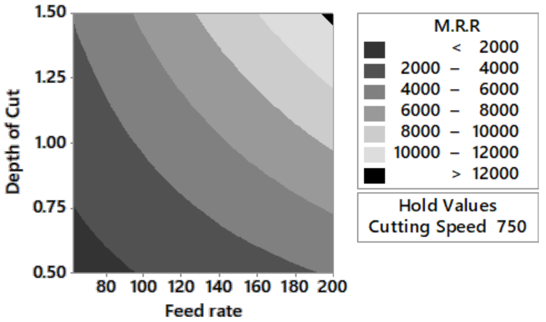

Fig 19(a). Contour plot of MRR for cutting depth vs. feed rate (f)

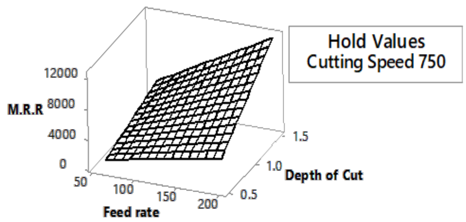

Fig 19(b). Response plot of MRR for cutting depth vs. feed rate (f)

Figures 20(a) and 20(b) shows 2D contour plot and 3D response of MRR for cutting depth and spindle speed (N). From Fig. 20, maximum values for MRR occurs at high values of cutting depth and high values of spindle speed (N).

Figures 21(a) and 21(b) shows 2D contour plot and 3D response plot of MRR for feed rate (f) and spindle speed (N). From Fig. 21, maximum values for MRR occurs at high values of spindle speed (N) and high values of feed rate (f).

4.5. Multiple Objective Optimization Using RSM

In the current work, four responses, i.e. cutting force (Fc), Ra, flatness and MRR obtained from the FE model, have been optimized simultaneously using desirability function optimization of the RSM. The individual desirability of output parameters combined using the concept of composite desirability into an overall value, D. In order to obtain optimum milling conditions, the responses should be in the optimum conditions. Fig 22 shows the multi objective optimization results using RSM. Values in the square brackets indicate the optimized values of parameters and the y-values, under each response, indicate the optimized values of each responses. If the composite desirability D value is close to one, implies the importance of responses. In this work, the composite desirability, D= 0.5779.

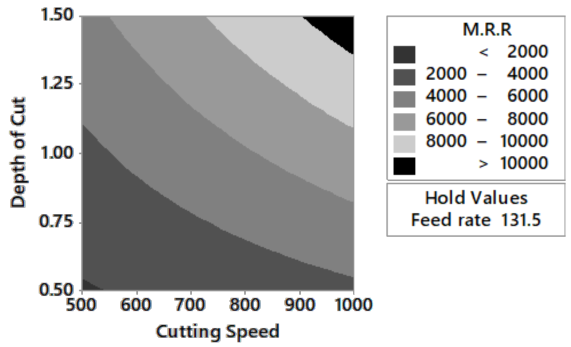

Fig 20(a). Contour plot of MRR for cutting depth vs. spindle speed (N)

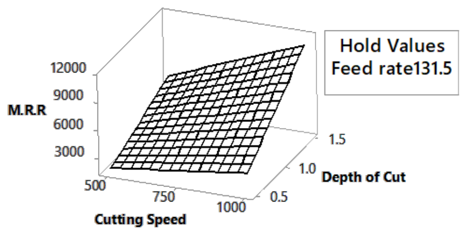

Fig 20(b). Response plot of MRR for cutting depth vs. spindle speed (N)

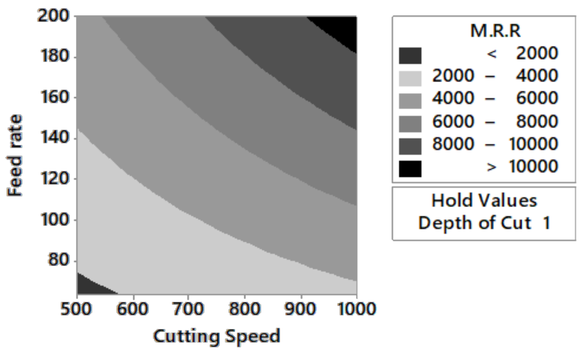

Fig 21(a). Contour plot of MRR for feed vs. spindle speed (N)

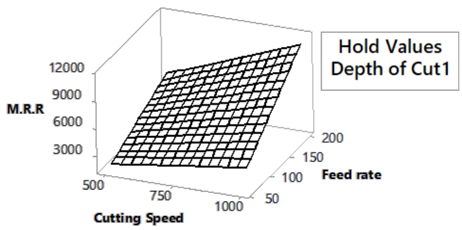

Fig 21(b). Response plot of MRR for feed vs. spindle speed (N)

4.6. Confirmation of results

Results are confirmed by running simulations in the validated model three times for optimized cutting conditions i.e. Cutting depth = 0.8636 mm, Spindle speed (N) = 1000 rpm, and Feed (f) = 200 mm/min. The responses, cutting force (Fc), Ra, flatness and MRR were measured and the mean value was found. The results are shown in Table 7.

Table 7. Confirmation of results

	MRR (mm^3/sec)	PEEQ	FLATNESS (*10^{-3}mm)	CUTTING FORCE (F_C) (N)
Optimized values	9598.365	0.7683	0.0404	4423.144
Simulation result	9513.634	0.7609	0.0460	4495.875
Percentage Error	0.882	0.9631	12.173	1.617

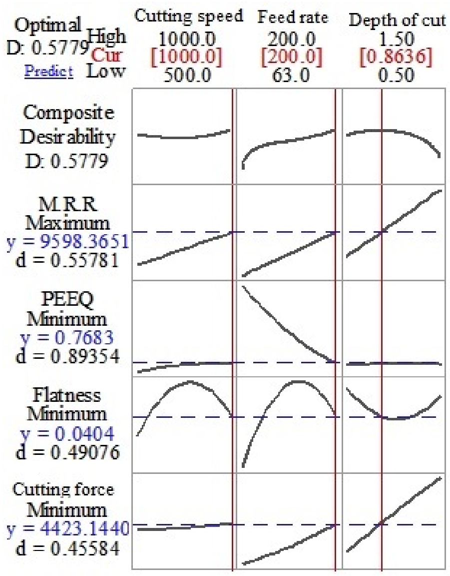

Fig 22. Optimization plot

5. Conclusions

The current work aimed at simultaneous minimization of cutting force, flatness, PEEQ and maximization of MRR in face milling of AISI 304 steel. A validated numerical model was developed and used in this paper. The significance of this research work is to help manufacturer and cutting tool designer to understand the nature of machining induced flatness and surface finish. In this work, the influence of milling parameters like, cutting depth, spindle speed (N) and feed (f) on responses such as, Ra, cutting force (Fc), flatness and MRR during face milling of AISI 304 steel using RSM was studied. Using Design of Experiments software, ANOVA were performed for each responses. Optimization of process was done using central design of RSM. Using composite desirability functions, the multiple objective optimization of milling was studied. Following are the important findings of this study:

- The developed numerical model can predict the output parameters effectively in face milling of AISI 304 steel.
- Feed rate and depth of cut significantly affect the cutting force.
- All the three cutting parameters, ie. Cutting Speed, Feed Rate and Depth of cut have significant effect on MRR.
- All the parameters have no significant influence on flatness.
- Feed rate has significant effect on PEEQ.
- An increase in cutting speed, feed rate and depth of cut significantly increases MRR.
- Cutting depth at 0.8636 mm, feed rate at 200 mm/min. and cutting speed at 1000 rpm yield optimum values of the output parameters, when multi objective optimization of all the responses considered simultaneously.
- Confirmation experiments were performed with optimum values obtained through RSM. The results show very close agreement which validates the significance of the developed model or the work.

Conflict of Interest

The author(s) declared no potential conflicts of interest with respect to the research, authorship and publication of this article.

Funding

The author(s) received no financial support for the research, authorship and publication of this article.

Nomenclature

N_c	Cutting Speed [rpm]	D_1, D_2, D_3, D_4, D_5	Damage Parameters
f	Feed rate [mm/min]	σ_m	Mean Stress [MPa]
doc	Depth of Cut [mm]	ρ	Density [kg/m^3]
$\bar{\sigma}$	Equivalent flow stress [MPa]	E	Young's Modulus [GPa]
A, B, C, n, m	Material Constants	υ	Poisson's Ratio
T_{melt}	Melting Temperature [^{0}C]	K	Thermal Conductivity [W/mK]
T_{melt}	Room Temperature [^{0}C]	C_p	Specific heat [J/g^{0}C]
$\dot{\varepsilon}_0$	Reference Strain Rate [1/s]	α	Thermal expansion [/^{0}C]
$\bar{\varepsilon}_{pl}$	Equivalent Plastic Strain	$PEEQ$	Equivalent Plastic Strain
$\dot{\bar{\varepsilon}}_{pl}$	Equivalent Plastic Strain Rate	MRR	Material Removal Rate [mm^3/sec]
$\bar{\varepsilon}_{oi}^{\,f}$	Initial Failure Strain	Fc	Cutting Force [N]

References

[1] Kannan, S., Baskar, N., Sureshkumar, B., Selection of Machining Parameters in Face Milling Operations for Copper Work Piece Material Using Response Surface Methodology and Genetic Algorithm, *All India Manufacturing Technology, Design and Research Conference*, 2014.

[2] Prajapati, V., Thakkar, K., Thakkar, S., Parikh, H., Study and Investigate Effects of Cutting Parameters in CNC Milling process for Aluminium alloy-8011H14 through Taguchi design method, *International Journal of Innovative Research in Science, Engineering and Technology*, 2, 2013, 3271-3276.

[3] Yasir, M., Ginta, T., Ariwahj, B., Alkali, A., Danish, M., Effect of Spindle speed (N) and Feed rate (f) On Ra of AISI 316L SS Using End-Milling, *ARPN Journal of Engineering and Applied Sciences*, 11, 2016, 2496-2500.

[4] Shaik, J., Srinivas, J., Optimal selection of operating parameters in end milling of Al-6061 work materials using multi-objective approach, *Mechanics of Advanced Materials and Modern Processes*, 3(5), 2017, 1-11.

[5] Balasubramanyam, N., Gnana Prakash, P., Palvannan, V., Yugandhar, M., Effect of Machining Parameters on Ra of End Milling, *International Journal for Research in Applied Science &Engineering Technology*, 3(2), 2015, 1-10.

[6] Vijay, S., Krishnraj, V., Machining parameters optimization in End milling ofTi-6Al-4V, *International Conference on Design and Manufacturing*, 2013, 1079-1088.

[7] Rameshkumar, K., Krishnakumar, P., Ramachandran, K.I., Machine Learning Based Tool Condition classification using AE

and Vibration data in a High Speed Milling Process Using Wavelet Features, *Intelligent Decision Technologies: An International Journal*, 12(1), 2018, 1-18.
[8] Kumar, A., Paswan, M.K., Optimization of Cutting Parameters Of AISI H13 with Multiple Performance Characteristics, *International Journal of Mechanical Engineering and Robotics Research*, 2(3), 2013, 45-54.
[9] Ninase, R.N., Khodke, P.M., Effect of Machining Parameters on Ra of Al-7075 Alloy in End Milling, *International Research Journal of Engineering and Technology*, 2(3), 2015, 1505-1508.
[10] Wathore, H.D., Adwani, P.S., Investigation of Optimum Cutting Parameters for End Milling of H13 Die Steel using Taguchi based Grey Relational Analysis, *International Journal of Scientific Engineering and Applied Science*, 1(4), 2015, 309-318.
[11] Kumbhar, A., Bhosale, R., Modi, A., Jadhav, S., Nippanikar, S., Kulkarni, A., Multi-objective Optimization of Machining Parameters in CNC End Milling of Stainless Steel 304, *International Journal of Innovative Research in Science, Engineering and Technology*, 4(9), 2015, 8419-8426.
[12] Marimuthu, K.P., Kumar, C.S.C., Prasada, H.P.T., Mathematical modelling to predict the residual stresses induced in milling process, *International Journal of Mechanical and Production Engineering Research and Development*, 8, 2018, 423-428.
[13] Rawangwong, S., Chatthonga, J., Boonchouytan, W., Burapa, R., An Investigation of Optimum Cutting Conditions in Face Milling Aluminum Semi Solid 2024 Using Carbide Tool, *Energy Procedia*, 34, 2013, 854-862.
[14] Rawang, S., Chatthong, J., Boonchouytan, W., Burapa, R., Influence of Cutting Parameters in Face Milling Semi-Solid AA 7075 Using Carbide Tool Affected the Ra and Tool Wear, *11th Eco-Energy and Materials Science and Engineering*, 56, 2014, 448-457.
[15] Lakshmi, V., Subbaiah, K., Modelling and Optimization of Process Parameters during End Milling of Hardened Steel, *International Journal of Engineering Research and Applications*, 2, 2012, 674-679.
[16] Shelar, A., Shaikh, A., Optimization of CNC Milling Process by using Different Coatings- A Review, *International Advanced Research Journal in Science, Engineering and Technology*, 4(1), 2017, 143-147.
[17] Pramod, M., Reddy, N.V., Talluru, V., Reddy, Y.G., Marimuthu, K.P., Coupled temperature displacement model to predict residual stresses in milling process, *IOP Conference Series: Materials Science and Engineering*, 225, 2017.
[18] Subramanian, N., Veerapriya, C., Optimization of process parameters in milling process for AISI 4340 steel by Taguchi method, *International Journal of Research and Engineering, Science and Technology*, 1(1), 2015, 13-19.
[19] Sheth, S., George, P.M., Experimental Investigation and Prediction of Flatness and Ra during Face Milling Operation of WCB Material, *Procedia Technology*, 23, 2016, 344-351.
[20] Moaz, H.A., Basim, A., Khidhir, M.N.M., Ansari, B.M., FEM to predict the effect of feed rate (f) on Ra with cutting force (Fc) during face milling of titanium alloy, *HBRC Journal*, 9, 2013, 263-269.
[21] Krishna, K.P., Sripathi, J., Vijay, P., Ramachandran, K.I., Finite Element Modelling and Residual Stress Prediction in End Milling of Ti6Al4Valloy, *IOP Conference Series: Materials Science and Engineering*, 149, 2016, 012154.
[22] Ramesh, A., Sumesh, C.S., Abhilash, P.M., Rakesh, S., Finite element modelling of orthogonal machining of hard to machine materials, *International Journal of Machining and Machinability of Materials*, 17(6), 2015, 543-568.
[23] Sumesh, C.S., Ramesh, A., Numerical Modelling and Optimization of Dry Orthogonal Turning of Al6061 T6 Alloy, *Periodica Polytechnica Mechanical Engineering*, 62(3), 2018, 196-202.
[24] Reimer, A., Fitzpatrick, S., Luo, X.C., Zhao, J., Numerical Investigation of Mechanical Induced Stress during Precision End Milling Hardened Tool Steel, *Solid State Phenomena*, 261, 2017, 362-369.
[25] Ducobu, F., Arrazola, P.J.E., Rivière, L., Ortiz, G., de Zarate, A., Filippia, M.E., The CEL Method as an Alternative to the Current Modelling Approaches for Ti6Al4V Orthogonal Cutting Simulation, *Procedia CIRP*, 58, 2017, 245-250.
[26] Rezaei, H., Sadaghi, M.H., Budak, E., Determination of minimum uncut chip thickness under various machining condition during micro milling of Ti-6Al-4V, *International Journal of Advanced Manufacturing Technology*, 95(5-8), 2018, 1617-1634.
[27] Aydin, M., Koklu, U., Identification and modelling of cutting forces in ball end milling based on two different finite element models with Arbitrary Lagrangian Eulerian technique, *International Journal of Advanced Manufacturing Technology*, 92(1-4), 2017, 1465-1480.
[28] Peng, Z., Li, J., Yan, P., Gao, S., Zhang, C., Wang, X., Experimental and Simulation research on micro milling temperature and cutting deformations of heat resistance stainless steel, *International Journal of Advanced Manufacturing Technology*, 95(5-8), 2018, 2495-2508.
[29] Gao, Y., Ko, J.H., Lee, H.P., 3D coupled Eulerian Lagrangian finite element analysis of end milling, *International Journal of Advanced Manufacturing Technology*, 98(1-4), 2018, 849-857.
[30] Pittala, G.M., Monno, M., 3D finite element modelling of face milling of continuous chip material, *International Journal of Advanced Manufacturing Technology*, 47(5-8), 2010, 543-555.
[31] Krasauskas, P., Kilikevičius, S., Česnavičius, R., Pačenga, D., Experimental analysis and numerical simulation of the stainless AISI 304 steel friction drilling process, *Mechanika*, 20(6), 2014, 590-595.
[32] Pimenov, D.Y., Guzeev, V.I., Mathematical model of plowing forces to account for flank wear using FME modeling for orthogonal cutting scheme, *International Journal of Advanced Manufacturing Technology*, 89(9-12), 2017, 3149-3159.
[33] Pimenov, D.Y., Experimental research of face mill wear effect to flat surface roughness, *Journal of Friction and Wear*, 35(3), 2014, 250-254.
[34] Pimenov, D.Y., Guzeev, V.I., Krolczyk, G., Mia, M., Wojciechowski, S., Modeling flatness deviation in face milling considering angular movement of the machine tool system components and tool flank wear, *Precision Engineering*, 54, 2018, 327-337.
[35] Grzenda, M., Bustillo, A., Semi-supervised roughness prediction with partly unlabeled vibration data streams, *Journal of*

Intelligent Manufacturing, 30(2), 2019, 933-945.
[36] Rodríguez, J.J., Quintana, G., Bustillo, A., Ciurana, J., A decision-making tool based on decision trees for roughness prediction in face milling, *International Journal of Computer Integrated Manufacturing*, 30(9), 2017, 943-957.
[37] Wojciechowski, S., Maruda, R.W., Nieslony, P., Krolczyk, G.M., Application of signal to noise ratio and grey relational analysis to minimize forces and vibrations during precise ball end milling, *Precision Engineering*, 51, 2018, 582-596.
[38] Wojciechowski, S., Wiackiewicz, M., Krolczyk, G.M., Study on metrological relations between instant tool displacements and surface roughness during precise ball end milling, *Measurement*, 129, 2018, 686-694.
[39] Wojciechowski, S., Maruda, R.W., Barranas, S., Nieslony, P., Krolczyk, G.M., Optimisation of machining parameters during ball end milling of hardened steel with various surface inclinations, *Measurement*, 111, 2017, 18-28.
[40] Chen, G., Ren, C., Yang, X., Jin, X., Guo, T., Finite Element Simulation of high speed machining of Titanium alloy (Ti-6Al-4V) based on ductile failure model, *International Journal of Advanced Manufacturing Technology*, 56, 2011, 1027-1038.
[41] Abaqus Inc. Analysis user's manual, Version 6.6 USA, 2006.